

REFERENCES

- ASCE. (2010). "Minimum Design Loads for Buildings and Other Structures." ASCE/SEI Standard 7-10.
- Brusiani, F., De Miranda, S., Patruno, L., Ubertini, F., & Vaona, P. (2013). On the evaluation of bridge deck flutter derivatives using RANS turbulence models. *Journal of Wind Engineering and Industrial Aerodynamics*, 119, 39-47.
- Chowdhury, A. G., & Sarkar, P. P. (2003). A new technique for identification of eighteen flutter derivatives using a three-degree-of-freedom section model. *Engineering Structures*, 25(14), 1763-1772.
- de Miranda, S., Patruno, L., Ubertini, F., & Vairo, G. (2014). On the identification of flutter derivatives of bridge decks via RANS turbulence models: Benchmarking on rectangular prisms. *Engineering Structures*, 76, 359-370.
- Den Hartog, J.P., 1956. *Mechanical Vibrations*. 4th ed. McGraw-Hill, New York
- Diana, G., Resta, F., Zasso, A., Belloli, M., & Rocchi, D. (2004). "Forced motion and free motion aeroelastic tests on a new concept dynamometric section model of the Messina suspension bridge." *Journal of wind engineering and industrial aerodynamics*, 92(6), 441-462.
- Gu, M., Zhang, R., & Xiang, H. (2000). Identification of flutter derivatives of bridge decks. *Journal of Wind Engineering and Industrial Aerodynamics*, 84(2), 151-162.
- Iwamoto, M., & Fujino, Y. (1995). Identification of flutter derivatives of bridge deck from free vibration data. *Journal of Wind Engineering and Industrial Aerodynamics*, 54, 55-63.
- Šarkić, A., Fisch, R., Höffer, R., & Bletzinger, K. U. (2012). Bridge flutter derivatives based on computed, validated pressure fields. *Journal of Wind Engineering and Industrial Aerodynamics*, 104, 141-151.
- Selvam, R. P., Govindaswamy, S., & Bosch, H. (2001). *Aeroelastic analysis of bridge girder section using computer modeling (No. MBTC FR-1095)*. University of Arkansas, Mack-Blackwell National Rural Transportation Study Center.
- Simiu, E., & Scanlan, R. H. (1996). *Wind effects on structures: fundamentals and applications to design*.
- Wikipedia (last access 24 October 2018): <https://en.wikipedia.org/wiki/Aeroelasticity>
- Wilcox, D. C. (1988). Multiscale model for turbulent flows. *AIAA journal*, 26(11), 1311-1320.

Experimental Study on Seismic Behavior of Scoured Pile-Group Foundations Considering Pile Uplift

Tengfei Liu¹; Xiaowei Wang, Ph.D., Aff.M.ASCE²; and Aijun Ye, Ph.D.³

¹Ph.D. Candidate, State Key Laboratory of Disaster Reduction in Civil Engineering, Tongji Univ., Shanghai 200092, China. E-mail: 15liutengfei@tongji.edu.cn

²Assistant Professor, Dept. of Civil Engineering, Hohai Univ., Nanjing 210098, China; Formerly Ph.D. Student, State Key Laboratory of Disaster Reduction in Civil Engineering, Tongji Univ., Shanghai 200092, China. E-mail: x.wang@hhu.edu.cn

³Professor, State Key Laboratory of Disaster Reduction in Civil Engineering, Tongji Univ., Shanghai 200092, China (primary author). E-mail: yeaijun@tongji.edu.cn

ABSTRACT

Scoured pile-group foundations, as one of the most vulnerable parts of bridges, can suffer inelastic deformations under earthquakes. Other than capacity-protection strategy, one alternative solution is to treat the scoured pile-group foundations as potential energy-dissipation components with limited ductility. To this end, the seismic behavior of scoured pile foundations should be evaluated carefully. In this study, to reveal the impact of pile uplift on the seismic behavior of scoured pile-group-foundations, quasi-static cyclic loading tests were conducted on two 2×2 RC square-pile foundation specimens with and without significant pile-uplift potentials. The hysteretic behavior, cap rotations, and pile damages were recorded. Dissipated seismic energy were also discussed. Test results reveal that the specimen with significant pile-uplift, compared with its counterpart, has flag-shaped hysteretic loops, indicating a pile-uplift failure mode. The seismic energy was mainly dissipated by the pile-soil interface friction, suggesting the effect of pile-uplift should be considered carefully.

Keywords: pile foundations; quasi-static test; pile uplift; seismic behavior; scour

INTRODUCTION

For bridges across rivers, pile foundations constructed in water may often undergo scour hazard, which is reported to be one of the most severe hazards causing bridge failures in the United States (Shirole and Holt 1991; Lagasse and Richardson 2001). For the seismic design of bridges, the pile-group foundation is generally one of the most vulnerable parts of bridges. For instance, plastic pile damages were reported in recent earthquakes (Bray et al. 2010; Ashford et al. 2011; Cubrinovski and Bray 2017). This becomes particularly challenging when bridges are subject to the scour hazard, because scour can cause degradations of foundation capacities (Achmus et al. 2010), pile-soil interface friction and alter seismic behavior of bridges. In this regard, full-embedded pile-group foundations that are originally designed based on the principle of capacity-protection (JSCE 2005; AASHTO 2011; MOHURD 2011) are probably subject to inelastic behavior under the effect of scour hazard.

Except for the capacity-protection design method mentioned above, an alternative solution to this issue is to treat scoured pile-group foundations as potential energy-dissipation components with limited ductility (ATC-32 1996). Considering this, the seismic behavior of scoured pile foundations should be well documented first. Relatively rare experimental and numerical studies (Chai and Hutchinson 2002; Rollins et al. 2005; Ye et al. 2011; Wang et al. 2016) had been done. Among them, hardly any research paid attention to the pile uplift behavior.

In this regard, quasi-static cyclic loading tests on two 2×2 RC pile foundation specimens in layered soils were conducted to reveal the influence of pile uplift on the seismic behavior of scoured pile-group-foundations. The pile-uplift effect is achieved through additional bending moments applied on caps that facilitate the rotation of pile-group foundations. Meanwhile, axial compressive loads were applied on both specimens through vertical hydraulic actuators. The plastic damages on piles, the hysteretic behavior of specimens, cap rotations and dissipated seismic energy were obtained. Test results indicate that specimen S-B, with additional moment on caps, showed distinct seismic pile-uplift failure mode, characterized as flag-shaped hysteretic loops, with lower lateral resistance and minor pile damages than its counterpart. Furthermore, pile uplift leads to greater lateral displacement of superstructures and lower dissipated seismic energy, meaning more attention is needed when evaluate the seismic behavior of laterally-loaded scoured pile foundations in future.

EXPERIMENTAL PROGRAM

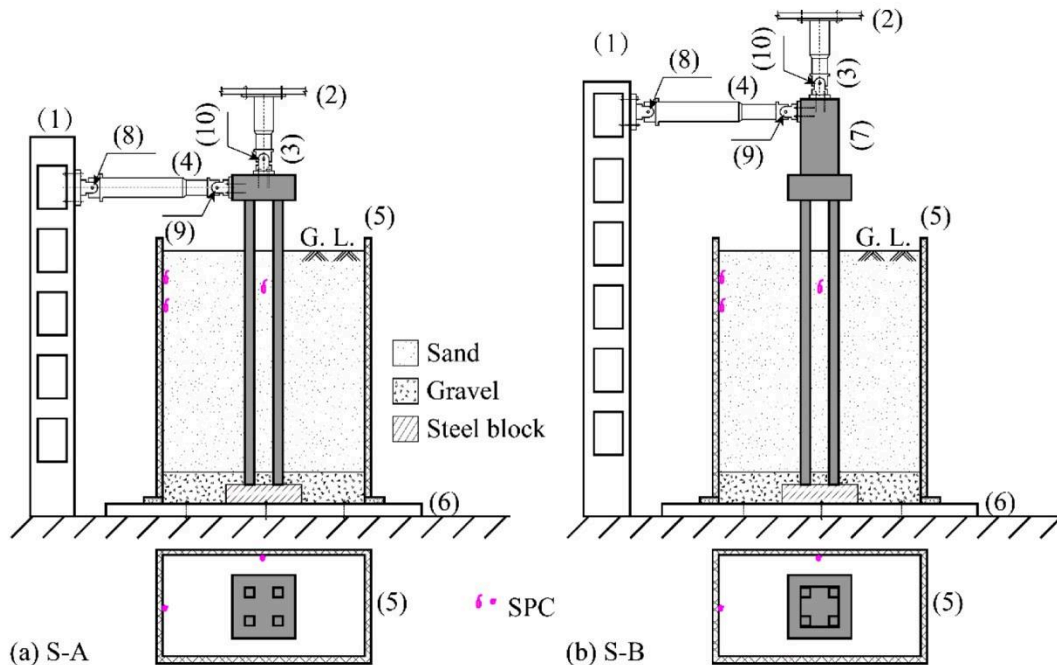
Test Setup

In this study, a pair of 2×2 RC pile foundation specimens were designed and fabricated to investigate the impact of pile uplift on seismic behaviors of scoured pile foundations. Note that the pile uplift behavior was achieved by considering additional bending moment acting on caps. Figure 1 (a) and (b) illustrate test setup schematics of S-A and S-B, respectively. As can be seen, each specimen consists of one square-section RC cap and four square-section piles with the same dimensions. Compared with its counterpart, specimen S-B has extra solid RC square-section pier above the cap to connect with actuators for loading. It is worth noting that the additional bending moment in specimen S-B can trigger a significant pile-uplift, as compared to the specimen S-A, in which a negligible pile-uplift may occur under lateral loads. In both cases, all piles are 4.50 m long and 0.15 m in widths (D). The aboveground height and embedded depth of piles were 0.80 m and 3.7 m, respectively. In S-B, the additional pier was 0.6 m (D_p)×0.6 m (D_p)×1.2 m (H). The soil profile includes 3.5-meter dry sand layer and 0.5-meter compacted gravel layer. Steel blocks were placed under specimens to control vertical settlements. The size of soil container is 3.2 m (L)×1.6 m (L)×4.2 m (H), ensuring the distances between specimens and soil container walls greater than 6 D and 3 D in longitudinal and perpendicular directions, respectively. Note that 3 soil pressure cells were glued on soil box walls to examine the boundary condition, which has also been verified by Wang et al. (2016). For simplicity, this part is not described below. Table 1 summarizes the layouts of both specimens in detail.

Specimen Materials

Both specimens were in situ cast and cured before test. Each pile was reinforced with four 12 mm diameter longitudinal bars and confined by several 8 mm diameter transverse loops. The concrete cover was 20 mm in thickness. The longitudinal and transverse reinforcement ratios were 2% and 1.8%, respectively. Note that the transverse reinforcement beneath cap-pile interface up to 2.0 meters was strengthened. The pile material properties are summarized in Table 2.

By weighing the test sand, the relative density of sand was determined to be 65%. The friction angle of sand was 31 degree obtained from direct shear test. Since the compacted gravel layer are placed just to increase vertical resistances of piles, no material property test was conducted herein. Table 3 lists the test sand properties.



(1) Reaction Wall; (2) Steel Frame; (3) Vertical Hydraulic Actuator; (4) Lateral Hydraulic Actuator; (5) Soil Box; (6) Concrete Base; (7) Pier; (8) Joint A (fixed); (9) Joint B (Free); (10) Joint C (Fixed).

Figure 1 Schematic Test Setup of (a)S-A and (b) S-B

Table 1 Specimen Layout Details (Unit: m)

Specimens	Pile		Cap		Pier	
	D	H	D _c	H _c	D _p	H _p
S-A	0.15	4.5	1.0	0.4	-	
S-B	0.15	4.5	1.0	0.4	0.6	1.2

Table 2 Pile Material Properties

Pile Material Parameters	Values
Concrete	
Uniaxial compressive strength (MPa)	42.1
Concrete Strain at peak strength	0.099
Longitudinal Steel	
Yield Strength (MPa)	542.4
Initial Elastic Modulus (MPa)	2.06×10^5
Peak Strength (MPa)	695.1
Transverse Steel	
Nominal Yield Strength (MPa)	320.1*

*: This value refers to strength at a strain of 0.2%.

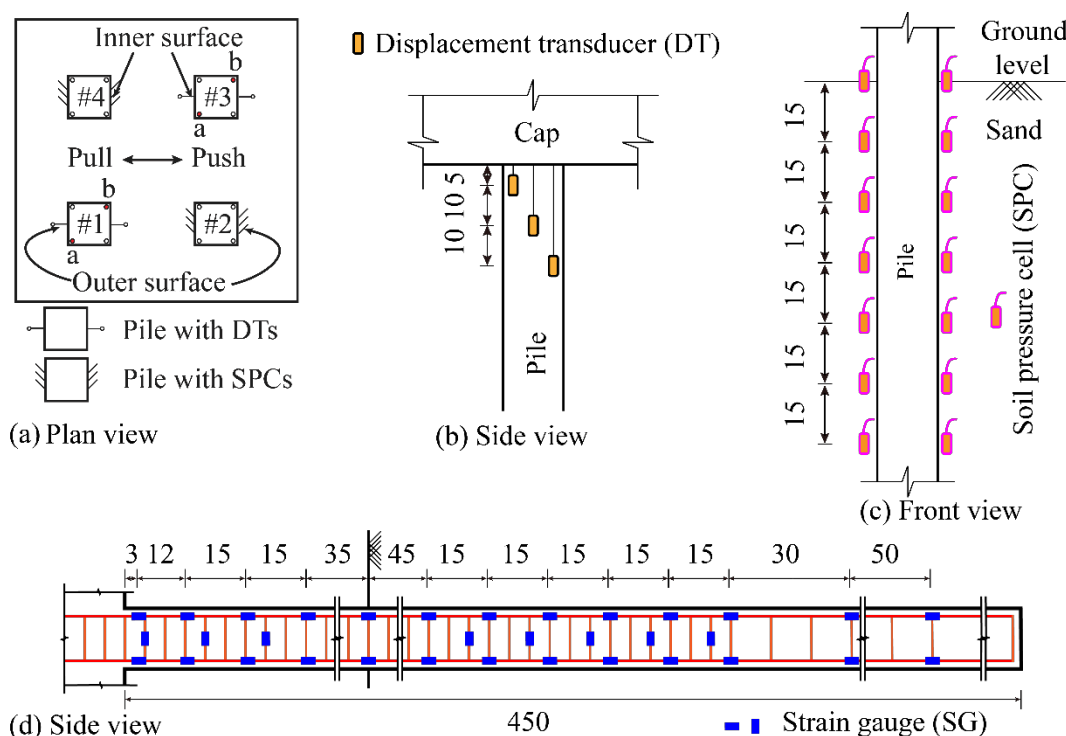
Table 3 Sand Properties

Sand Physical Parameters	Values
Unit Weight (kN/m^3)	15.6
Relative Density, D_r (%)	65
Friction Angle (deg)	31

Instruments

Figure 2 and Figure 3 present the instrumental arrangements on piles and caps (piers) in the test, respectively. In each case, half piles are instrumented with displacement transducers on opposite sides, as shown in Figure 2 (b), to calculate mean cross-section curvature in pile head regions, as depicted in Wang et al. (2016). Soil pressure cells are utilized on the other half piles to monitor soil reactions along piles during tests (see Figure 2 (c)). In Figure 2 (a), it should be noted that longitudinal bars labeled with red points and their corresponding transverse loops are glued with strain gauges to obtain pile curvature distribution (see Figure 2 (d)), consistent with Wang et al. (2016).

To record the cap rotation behavior, one inclinometer was glued on top of RC caps in both cases. Furthermore, four displacement transducers were connected with RC caps to monitor the lateral displacement history in each specimen. It is also worth noting that, in S-B, one extra displacement transducer was employed on the pier.

**Figure 2 Instruments of piles**

Loading Protocol

For each specimen, the constant vertical load was applied via vertical hydraulic jack to ensure 5% axial load ratio on each pile, with the lateral loading displacement-controlled. Figure 4 presents the lateral loading displacement histories for both specimens. Note that in S-A, the

horizontal hydraulic actuator was connected to the cap center for lateral loading while it was applied on the RC pier 1.2-meter level above the cap center, as shown in Figure 1. The lateral loading ended at 170 mm and 230 mm for S-A and S-B, respectively.

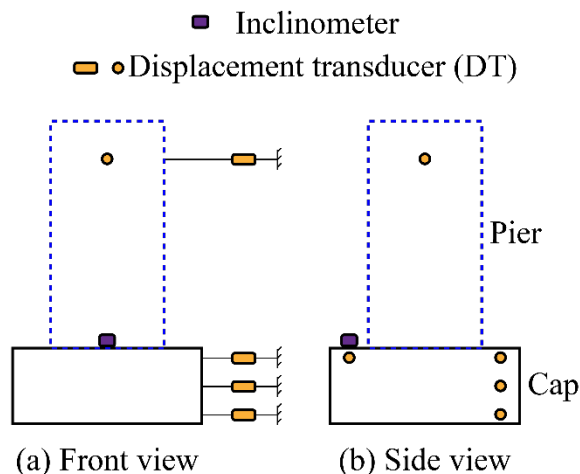


Figure 3 Instruments of caps (and piers, only in S-B)

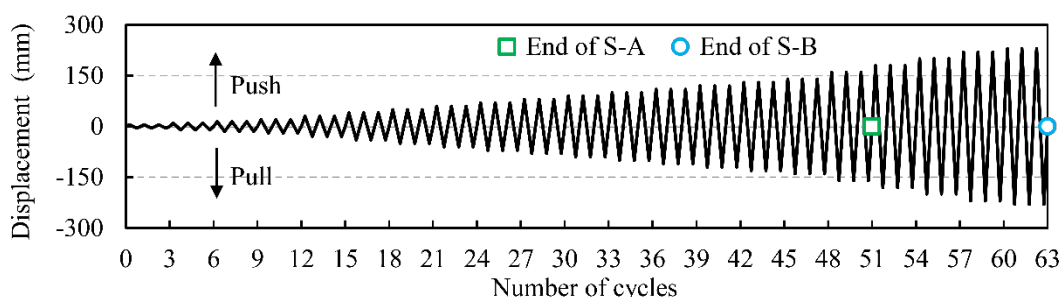


Figure 4 Displacement histories of specimens

OBSERVED PILE DAMAGES

Figure 5 shows the posttest pile damages on aboveground piles in both cases. It is obvious that in S-A, the aboveground pile damage is severe, featured with several wide horizontal concrete cracks penetrating four pile sides and the spalling of concrete cover. Meanwhile, pile damages are mainly distributed at pile heads ranging from cap-pile interface up to 1D-length regions. However, compared with S-A, fewer and much minor concrete cracks were detected at pile head regions in S-B, all of which occurred before the loading displacement level of 40 mm, indicating that the concrete damage only developed to a limited extent with increasing lateral loading.

After tests, underground pile damages from specimens S-A and S-B are detected, as illustrated in Figure 6 (a) and (b), respectively. For both cases, wide concrete cracks along pile-shaft beneath the ground level seems to reveal flexural failure mode, and the same embedded depth (85 cm) of most severe underground pile damages was observed. Additionally, S-B suffers less severe underground pile damages.

In expectation, with bending moment applied on caps, S-B should suffer less severe pile damages at pile heads, where the bending moment of pile section induced by lateral loading was greatly offset by the predesigned moment. On the other hand, underground pile damages from S-

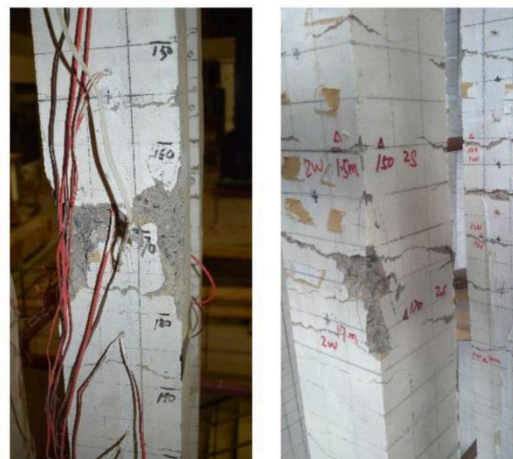
B should be more severe and shallower after test, since the maximum bending moment on piles beneath ground was strengthened by the predesigned additional moment on caps. The gap between theoretical analysis and test results indicates the soil-pile-interaction was influenced by the additional moment on caps, with lower gradient of soil reaction on piles than that S-A. Combined with the test phenomena, the explanation is the pile uplift behavior.



(a) S-A

(b) S-B

**Figure 5 Observed aboveground pile damages of pile specimens
(Courtesy of Prof. Aijun Ye and Mr. Tengfei Liu)**



(a) S-A

(b) S-B

**Figure 6 Underground pile damages of specimens
(Courtesy of Prof. Aijun Ye and Mr. Tengfei Liu)**

RESULTS AND DISCUSSION

Lateral Displacement Versus Lateral Load

From the lateral force-displacement relationship recorded by horizontal hydraulic actuator, the global behavior of each specimen was easily ascertained. Figure 7 plots the hysteretic hoops for specimens S-A and S-B. It can be seen that the pile-foundation specimen with or without additional bending moment on caps behaved totally different. For S-A, the hysteretic loop is plump and spindle-shaped, consistent with typical flexural bending failure mode of RC members.

At the early loading stage, the soil-pile system remains elastic, featured with approximately linear relationship between lateral load and displacement, then the inelastic pile behavior leads to spindle-shaped lateral load-deflection loops.

On the other hand, though hysteretic loops of specimen S-B are also plumped, the shape of them is like flag. Before reaching the lateral displacement of 30 mm, similar linear lateral load-displacement is also reached, after which the hysteretic loop became flag-shaped, feature with little difference in maximum lateral load between displacement levels and the apparent displacement slippage in unloading stages. Combined with the observed pile damages, it should be concluded that the specimen S-B shows a different failure mode of pile uplift, while the flexural failure mode of piles (see Figure 6 (b)) was secondary.

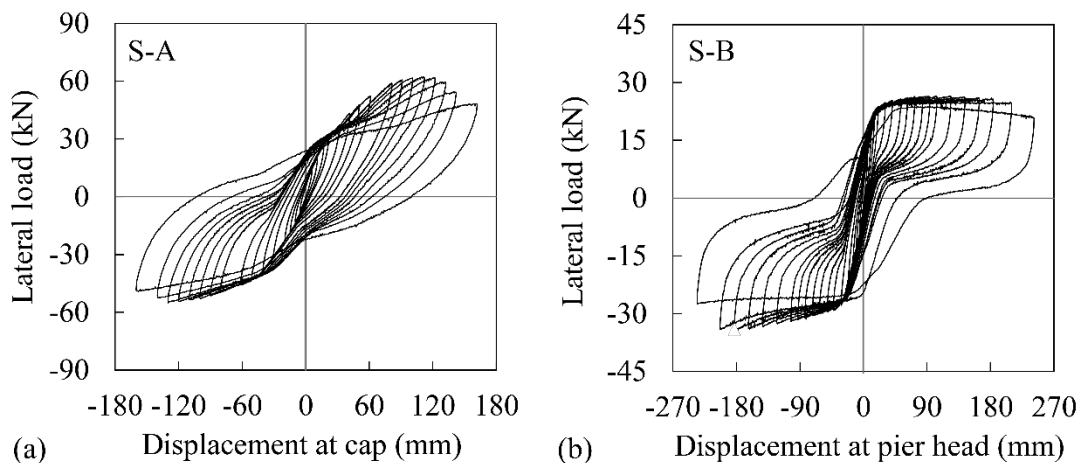


Figure 7 Hysteretic loops of specimens

Base on the hysteretic loops in both cases, the backbone curves of later load-displacement diagram are obtained, as shown in Figure 8. In general, both backbone curves are S-shaped. More specific, the peak lateral resistance in S-B was 48 percent lower than S-A in average (in push and pull directions) and larger loading displacement at peak lateral load was measured in S-B. According to this, it can be concluded that the pile uplift behavior can diminish the lateral resistance of soil-pile system heavily.

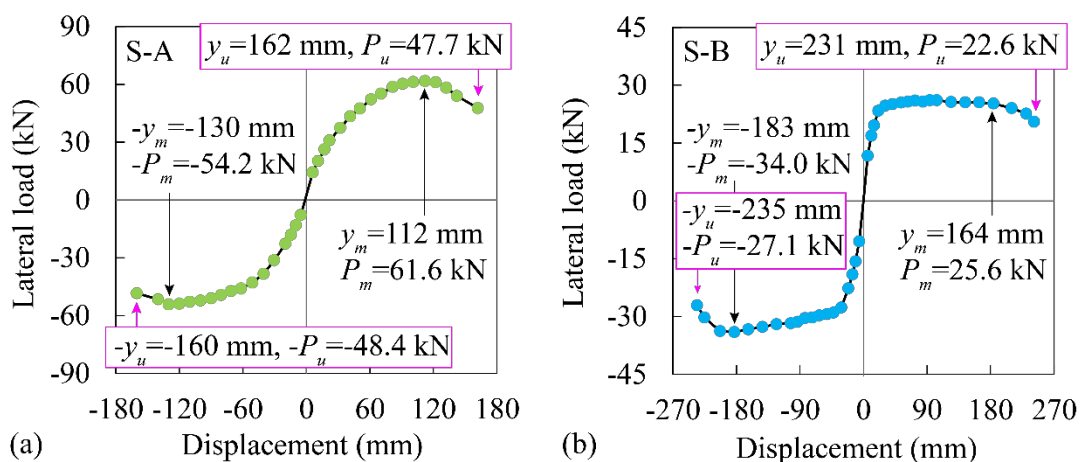


Figure 8 Backbone curves of specimens

Lateral Displacement Versus Cap Rotation

For bridges, the residual lateral displacement of superstructures induced by foundation rotation can be sizeable. To ensure the seismic performance of bridge structures under earthquakes, the foundation rotation should be evaluated and controlled carefully. Figure 9 illustrates the backbone curves of cap rotation versus lateral loading displacement for the pair of specimens in the test. In general, the cap rotation increases linearly with lateral loading displacement for both specimens.

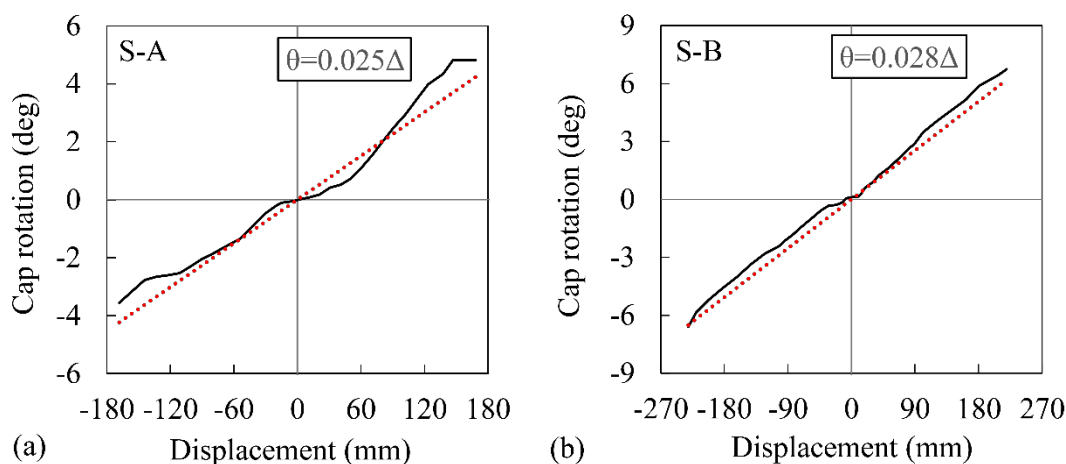


Figure 9 Cap rotation of specimens

More specific, with additional bending moment, the specimen S-B owns more rapid growth in cap rotation with the same lateral loading displacement than its counterpart, specimen S-A, indicating the pile uplift behavior can cause larger foundation rotation and greater lateral displacement at pier heads after earthquakes. In terms of limiting the displacement of bridge superstructures, pile uplift is one detrimental issue and needs more consideration in future.

Seismic Energy Dissipation

The seismic energy dissipated by the soil-pile system for S-A and S-B can be obtained by calculating the area of lateral displacement versus lateral load of specimens. The accumulative dissipated seismic energy absorbed by specimens S-A and S-B along with the lateral loading displacement is presented in Figure 10 (a), with their corresponding equivalent damping ratios at each loading level shown in Figure 10 (b). Note that the equivalent damping ratio is achieved based on the method proposed by Chopra (2007).

Since RC caps in both specimens and the pier in S-B remains elastic as expected, the seismic energy is mainly dissipated by plastic pile damages or the pile-soil interface friction. It can be seen that, compared with its counterpart, more seismic energy is absorbed in S-A. This can be explained by the more severe pile damages detected in S-A than S-B during the test. Since no apparent pile-uplift was observed during the test, the seismic energy was mainly dissipated by pile damages. With increasing lateral loading displacements, piles suffered plastic damages more rapidly and a nonlinear trend on the energy dissipated along the lateral loading displacement is expected, as shown in Figure 10 (a). However, in S-B, as discussed before, the spindle-shaped hysteretic loops indicates the dissipated seismic energy mainly lies in the pile-soil interface friction induced by pile uplift. So an approximately linear relationship between seismic energy

and lateral loading displacement is reached considering pile uplift.

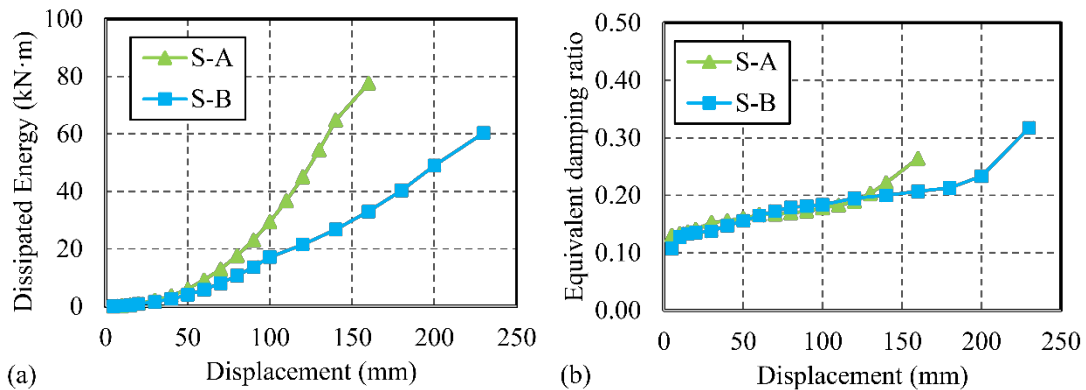


Figure 10 Seismic energy dissipation of specimens

As plotted in Figure 10 (b), the equivalent damping ratio of both specimens increased gradually from 0.10 to about 0.30 with the loading displacement, indicating the enhance of energy dissipating capacity along with lateral loading. Though S-A absorbed more energy than S-B (see Figure 10 (a)), the difference of equivalent damping ratio for S-A and S-B are rather small before the lateral displacement reaches 140 mm, indicating the specimen S-B also has high efficiency in energy dissipation with pile-uplift behavior. Compared with specimen S-A, the drops of accumulative energy absorbed by S-B under the same displacement levels mainly lie in the decrease of lateral capacity of soil-pile system.

CONCLUSIONS

In this study, quasi-static lateral loading tests on a pair of 2×2 scoured RC pile foundation specimens were conducted, emphasized in the impact of pile-uplift on the seismic behavior of pile foundations. Based on the test observation and analysis on the global hysteretic behavior, cap rotation and energy-dissipating capacity of each specimen, main conclusions can be drawn:

- (1) Additional bending moment on pile caps can lead to pile-uplift behavior, which should not be ignored when evaluating the seismic performance of pile specimens.
- (2) Less severe aboveground and underground pile damages were detected in specimen S-B, along with the flag-shaped hysteretic loops, indicates pile uplift dominates the failure mode of S-B over typical flexural failure mode.
- (3) Pile uplift leads to much lower lateral resistance of pile foundations, larger cap rotation and loss of energy-dissipation capacity, although nearly the same equivalent damping ratio was obtained in comparison with no pile uplift behavior. The effect of pile-uplift should be paid more attention in seismic evaluations of laterally loaded pile foundations.

ACKNOWLEDGEMENT

The financial support provided by the National Natural Science Foundation of China under Grant No. 51778469 is gratefully acknowledged.

REFERENCES

AASHTO (American Association of State Highway and Transportation Officials). (2011). *Guide Specifications for LRFD Seismic Bridge Design*. Washington D.C.